HILT: A Heavy Ion Large Area Proportional Counter Telescope for Solar and Anomalous Cosmic Rays

B. Klecker, D. Hovestadt, M. Scholer, H. Arbinger, M. Ertl, H. Kästle, E. Künneth, P. Laeverenz, E. Seidenschwang, J. B. Blake, N. Katz, and D. Mabry

Abstract— **The HILT sensor has been designed to measure heavy ion elemental abundances, energy spectra, and direction of incidence in the mass range from helium to iron and in the energy range 4 to 250 MeV/nucleon. With its large geometric factor of 60 cm^{2}sr the sensor is optimized to provide compositional and spectral measurements for low intensity cosmic rays, i.e. for small solar energetic particle events and for the anomalous component of cosmic rays. The instrument combines a large area ion drift chamber–proportional counter system with two arrays of 16 Li-drift solid state detectors and 16 CsI crystals. The multi dE/dx-E technique provides a low background mass and energy determination. The sensor also measures particle direction. Combining these measurements with the information on the spacecraft position and attitude in the low altitude polar orbit, it will be possible to infer the ionic charge of the ions from the local cutoff of the Earth's magnetic field. The ionic charge in this energy range is of particular interest because it provides unique clues to the origin of these particles and has not been investigated systematically so far. Together with the other instruments on board SAMPEX (LEICA, MAST, and PET), a comprehensive measurement of the entire solar and anomalous particle population will be achieved.**

I. Introduction

THE HILT (Heavy Ion Large Telescope) sensor, together with the LEICA sensor, was originally developed for a Get-Away-Special Payload (G-0335) to measure solar and anomalous cosmic rays in a high inclination shuttle orbit at solar minimum conditions [1]. The payload was scheduled for a series of STS flights starting in 1986. However, because of the Challenger accident, it was delayed and finally flown only once on the space shuttle mission STS-28 in August 1989. In a collaborative effort of the Max-Planck-Institut für Extraterrestrische Physik and the Aerospace Corporation, the HILT sensor has been modified to extend the range of elements and energies covered. The measurements now include heavy ions from helium to iron in the energy range from 4 to 250 MeV/nucleon. The sensor thus covers the maximum intensity of the anomalous component of cosmic rays and the medium energy range of solar energetic ions. The sensor utilizes a large area ion drift chamber, two position sensitive proportional counters, an array of 16 silicon solid state detectors and a CsI crystal unit to determine the nuclear charge, the energy, and the direction of ions entering the telescope. In the low altitude ($\approx$600 km) polar orbit of SAMPEX, this information will be used to infer the ions' ionic charge from the local cutoff of the magnetic field of the Earth.

Manuscript received August 3, 1992; revised January 25, 1993. This work was supported in part by DARA with Contract 50 OC 90021 and at The Aerospace Corporation by the NASA Cooperative Agreement 26979B.

B. Klecker, D. Hovestadt, M. Scholer, H. Arbinger, M. Ertl, H. Kastle, E. Kunneth, P. Laeverenz, and E. Seidenschwang are with the Max-Planck-Institut für Extraterrestrische Physik, W-8046 Garching bei München, Germany.

J. B. Blake, N. Katz, and D. Mabry are with The Aerospace Corporation.

IEEE Log Number 9208070.

II. Scientific Objectives

A. Solar Energetic Particles

During the last few years it has been recognized that solar energetic particle events (SEP) can be divided into two classes, based on the time scale of the electromagnetic emissions of their associated flares. SEP events associated with impulsive flares have mostly low particle intensities, high ^{3}He/^{4}He flux ratios, enhanced abundances of heavy elements, charge states indicative of heated flare plasma ($\approx 10^7$ K), high electron to proton flux ratios and high ratios of solar (interacting or trapped) to interplanetary (escaping) protons. The SEP events associated with gradual flares are characterized by large particle intensities in interplanetary space, low ^{3}He/^{4}He ratios, low electron to proton flux ratios, low ratios of solar to interplanetary proton intensities and charge states indicative of typical (2×10^6 K) coronal temperatures (e.g., [2] and references therein). Due to the limited collecting power of the instrumentation previously flown, composition and energy spectra for impulsive events have been studied only over a small energy range (e.g., [3], [4]). HILT, with its large geometric factor of 60 cm^{2}sr, will provide spectral and compositional information in particular for the low intensity events associated with impulsive flares. At high flux levels (>5 protons/cm^{2}s sr MeV/n at 5 MeV) pulse pile-up and accidental coincidences will degrade the performance of the instrument. However, flux levels exceeding this value are observed in interplanetary space only during very large, shock associated energetic particle events. However, with the four instruments of the SAMPEX payload a comprehensive measurement of the entire SEP population will be achieved (see also [5], [6]).

The large temperature differences as derived from heavy ion charge states observed in impulsive and gradual flares [7] show that the charge state measurements provide crucial

information. So far charge state measurements have been obtained only at energies <3 MeV/nucleon during a limited time period on ISEE-3 [8]. In the low altitude polar orbit of SAMPEX, it will be possible to extend these studies using the geomagnetic cutoff as described below.

B. Anomalous Component of Cosmic Rays

The anomalous component of cosmic rays (ACR) has been studied extensively since its discovery in the 1972–1977 solar minimum. In the energy range below ≈ 50 MeV/nucleon, at least six elements have been found (He, C, N, O, Ne, Ar) whose energy spectra show anomalous increases in flux above the quiet time galactic cosmic ray spectrum and whose composition is different from the solar or galactic cosmic ray composition [9]. There have been a number of models proposed to explain the ACR component. The most plausible theory for the origin of the ACR identifies neutral interstellar gas as the source material (Fisk *et al.* [10]). The neutral particles, after penetrating into the inner heliosphere, are ionized by solar UV radiation or by charge exchange reactions with solar wind protons. After ionization, the now singly charged ions are picked up by the interplanetary magnetic field and carried with the solar wind to the outer heliosphere. There the ions are accelerated to high energies, possibly at the solar wind termination shock [11]. A unique prediction of the model of Fisk *et al.* is that the anomalous cosmic rays should be singly ionized. Although indirect evidence for low charge states of the ACR has been found in many investigations (e.g., [12], [13]), results from a more direct measurement using the transmission of the Earth's magnetic field are sparse [14], [15]. It was only recently that a more systematic study of ACR oxygen charge states was started in a collaborative effort of many institutions [16]. The large collecting power of HILT and MAST [17] combined with an accurate measurement of time, position, and particle direction should overcome many of the difficulties encountered previously and provide definitive measurements of the charge state of oxygen and the less abundant ions of anomalous cosmic rays.

Recently, the discovery of anomalous cosmic ray oxygen trapped in the Earth's magnetosphere after charge exchange at low altitudes has been reported [18]. The low altitude polar orbit of SAMPEX will provide an excellent opportunity to study this newly discovered trapped component in great detail and to extend the present measurement of trapped oxygen to the less abundant ions.

C. Determination of Ionic Charge States

The geomagnetic cutoff can be used to infer the ionic charge of heavy ions. The cutoff rigidity, R_c, depends in general on the location in the magnetic field of the Earth and on the direction of the particle. The local cutoff R_c can be computed by using a model of the magnetic field of the Earth and trajectory tracing techniques. The particle rigidity, R, depends on kinetic energy per nucleon (T), mass (A), total energy per nucleon ($T + E_0$), and ionic charge (Q) as

$$R = T^{0.5*}(T + 2^*E_0)^{0.5*}A/Q\,.$$

Thus, after determining T and A from the measurement, an upper limit for the ionic charge Q can be obtained from the requirement $R > R_c$:

$$Q < T^{0.5}(T + 2^*E_0)^{0.5*}A/R_c\,.$$

For solar energetic particle events, the particle tracing technique can be complimented by the direct determination of the local cutoff rigidity from the cutoff in the proton spectrum, since the ionic charge is known in this case.

III. Instrument Description

The HILT sensor determines the mass, kinetic energy, and direction of particles entering the aperture by measuring the energy loss in a proportional counter–ionization chamber system and the residual energy in an array of 16 solid state detectors and a CsI crystal unit. A view of the sensor and analog and digital electronic in flight configuration is shown in Fig. 1. The instrument characteristics are summarized in Table I. The schematic diagram of HILT in Fig. 2 shows the main sensor components: a three-element ion drift chamber with thin aluminum entrance window (40 μg/cm^2), followed by an array of 16 solid state detectors (SSD) and 16 CsI scintillation counters which are embedded in a plate of PERSPEX material and viewed by four light sensitive silicon diodes. The entrance foil serves as part of the gas enclosure and, in combination with two additional aluminum foils ($2 \times 20\,\mu$g/cm^2), as a shield against micrometeoroid impacts. The entrance foils are protected by an acoustic cover (see Fig. 1) that can be opened and closed after launch.

A. Principle of Operation

The element or mass analysis is based on the combination of a multi dE/dx measurement in the position-sensitive proportional counter and ionization chamber system with the measurement of residual energy in the SSD detector array and the CsI crystal unit. The direction of incidence is derived from two position measurements as described below. With the information of particle energy, mass, and direction, in combination with the spacecraft position and attitude in the low altitude polar orbit, it will be possible to infer the ionic charge of the ions from the local cutoff of the Earth's magnetic field.

B. The Ion Drift Chamber—Proportional Counter System

The drift chamber–proportional counter system consists of three sections (Fig. 2). Electrons generated along the path of incoming ions drift in the electric field (85 V/cm) of the chamber to the front proportional counter (section I, PCF), to a charge collecting plate (section II, IC), and to the rear proportional counter (section III, PCR). The drift field is generated by a set of parallel wires (Mo, diameter 100 μ, spacing 5 mm) enclosing the drift chamber. In order to improve the homogeneity of the drift field near the wires, the inner layer of wires is enclosed by a second layer at a distance of 2 cm (see Fig. 2, note: only the top and bottom layers of wires are shown). In the first and third section of the drift chamber

TABLE I
HILT INSTRUMENT CHARACTERISTICS

Energy Range	Helium I	4.3–9.0	MeV/nuc (^{4}He)	PC-SSD coincid.
	Helium II	9.0–38	MeV/nuc (^{4}He)	PC-SSD-CsI coincid.
	Heavy Ion I	8.2–42	MeV/nuc (^{16}O)	PC-SSD coincid.
	Heavy Ion II	42.–220	MeV/nuc (^{16}O)	PC-SSD-CsI coincid.
Elemental Resolution (ΔZ)				
PC-SSD coincidence		0.3 FWHM	He < 9 MeV/n	
		0.3 FWHM	C, N, O < 42 MeV/n	
		0.6 FWHM	Fe < 75 MeV/n	
PC-SSD-CsI coincidence		0.5 FWHM	C, N, O > 42 MeV/n	
SSD-CsI coincidence		0.8 FWHM	C, N, O > 42 MeV/n (High Energy Mode)	
Mass Resolution (ΔA)		0.6 FWHM	He < 9 MeV/n	
View Angle		68 × 68	degree full angle	
Sensitive SSD area		159	cm^2	
Geometrical Factor		60	cm^2 sr	
Total Mass		22.8	kg including Isobutane supply	
Isobutane Counter Gas		7.2	kg	
Power		5.7	W at 40000 counts/s	
Telemetry		800	bps nominal allocation	

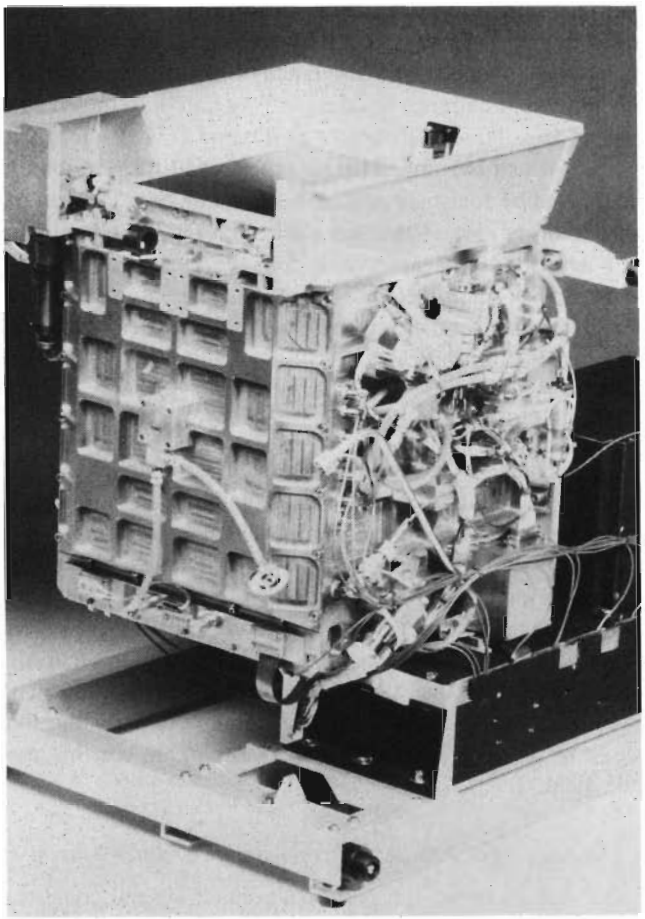

Fig. 1. HILT sensor with protective cover (closed), Isobutane system (right), and electronic box in flight configuration.

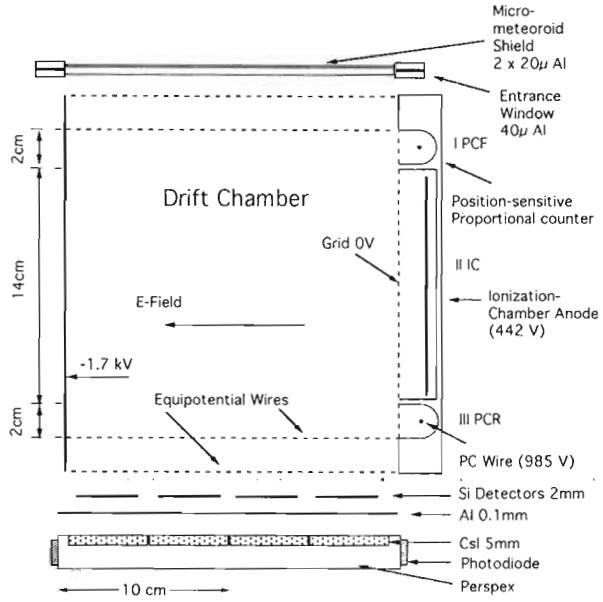

Fig. 2. Schematic cross section of HILT sensor.

energy loss and position of the ions are determined by two position-sensitive proportional counters with triangular shaped cathodes, the center element is operated as an ionization chamber and provides a third energy loss measurement. The energy loss of ions in all three sections is pulse height analyzed. The triple dE/dx measurement, in combination with the determination of the residual energy of the ions, provides a low background identification of ion type and energy in the mass range from helium to iron. In addition to the nuclear charge (element) resolution, the sensor also provides mass identification capability for helium (see also Table I).

The signals of the triangular shaped cathodes of the proportional counters are also pulse height analyzed. The ratios of the position and energy signal are a direct measure of the position along the proportional counter axis. In section I also the time elapsed between the response of the SSD's and the anode of PCF, i.e. the drift time of electrons generated along the track of incoming ions, is determined. Thus, drift time and position response of PCF provide two coordinates for the incoming ions at the top plane of the sensor. At the bottom plane the position response of PCR and the information on the detector row triggered by the incoming particles provide the other two coordinates. The trajectory of the incoming ions can be determined from these four coordinates The accuracy of the determination of the incident angle is limited by the diameter of the detectors and the energy and position response of the

TABLE II
HILT RATE DATA CHARACTERISTICS

Rate Acronym	Time Resolution (s)	Rate Type	Ion	Energy Range (MeV/Nucleon)	Geometry Factor (cm^2sr)
HE1	6	Coincidence	He	4.3–9	60
HE2	6	Coincidence	He	9.0–38	60
HZ1	6	Coincidence	$Z \geq 6$	8.2–42 (for ^{16}O)	60
HZ2	6	Coincidence	$Z \geq 6$	42.–220 (for ^{16}O)	60
HZ1*	6	Coincidence	$Z \geq 1$	5.–22 (for ^{1}H)	60
HZ2*	6	Coincidence	$Z \geq 1$	22.–60 (for ^{1}H)	60
SSD1	24	Single	$Z \geq 1$	> 5 (for ^{1}H)	15
SSD2	24	Single	$Z \geq 1$	> 5 (for ^{1}H)	15
SSD3	24	Single	$Z \geq 1$	> 5 (for ^{1}H)	15
SSD4	24	Single	$Z \geq 1$	> 5 (for ^{1}H)	15
PCFE	48	Single	$Z \geq 1$***	2.5–8 (for ^{1}H)	630
PCRE	48	Single	$Z \geq 1$***	2.5–8 (for ^{1}H)	190
IK	48	Single	$Z \geq 2$	3.0–9 (for ^{4}He)	300**
CsI	48	Single	$Z \geq 1$	22–60 (for ^{1}H)	105
HSSD1	0.1	Single	$Z \geq 1$	> 4 (for ^{1}H)	15
HSSD2	0.1	Single	$Z \geq 1$	> 4 (for ^{1}H)	15
HSSD3	0.1	Single	$Z \geq 1$	> 4 (for ^{1}H)	15
HSSD4	0.1	Single	$Z \geq 1$	> 4 (for ^{1}H)	15
HPCRE	0.1	Single	$Z \geq 1$***	2.5–21 (for ^{1}H)	190
HIK	0.1	Single	$Z \geq 1$	2.5–7 (for ^{1}H)	300**

* High Energy Mode
** energy dependent
*** efficiency for electrons at 0.6 MeV: $2*10^{-4}$

proportional counters and is typically 5° for $Z \geq 6$ ions at ≤ 40 MeV/nucleon. The trajectory information will be used for a path length correction of the energy loss measurement in the proportional counter–ionization chamber system to improve the elemental resolution of the sensor.

C. The Isobutane Regulation System

The drift chamber–proportional counter system operates with Isobutane at a pressure of 100 mbar (at 20°C). The density of the Isobutane is actively controlled by a gas regulation system consisting of a thermally controlled valve, a small ionization chamber with built-in ^{241}Am radioactive source (Alphatron), and regulation electronics. The volume of the Alphatron is directly connected to the sensor volume and the current from the ^{241}Am source is used in the regulation electronics for the control of the Isobutane in- flow by opening or closing the thermal valve. The Isobutane outflow can be controlled by a motor driven vent valve and flow regulation valve. The gas supply consists of 7.2 kg of liquid Isobutane, stored in one cylindrical aluminum–kevlar composite tank in the center of the spacecraft, and is sufficient for a continuous operation of 3 years. Similar regulation systems have been successfully flown on several MPE experiments for the IMP-7/8, S3-2, and ISSE-1/3 missions.

D. The Solid State Detector Array

Low energy ions are stopped in one of 16 circular Li-drift silicon solid state detectors. The thickness of the detectors is 2 mm and the sensitive area is 995 mm^2. The detectors are arranged in an 4×4 array with one row of four detectors connected to one amplifier chain. In addition to the pulse height analyzed energy signal the information on the particular row triggered by an ion is transmitted with the pulse height information. The total sensitive area and the sensor geometry result in a geometric factor of 60 cm^2sr for the coincidence measurement (see also Table II).

E. The CsI Crystal Array

High energy ions penetrating the solid state detectors are stopped in a set of 16 circular CsI crystals of 5 mm thickness and 46 mm diameter which are arranged behind the SSD array. The CsI signal is used to define low energy rates (CsI in anticoincidence) and high energy rates (PC-SSD-CsI coincidences, see also Tables I and II) for helium and $Z \geq 6$ ions. The CsI coincidence measurement extends the energy range of the sensor to 250 MeV/nucleon (for neon), however, without an anticoincidence measurement in the high energy section. The crystals are embedded in a rectangular plate (PERSPEX) of 2 cm thickness and are viewed by four light-sensitive silicon detectors. Due to limitations in the energy resolution of the CsI unit and the smaller signals in the IC-PC system for high energy ions the directional and elemental resolution is reduced, compared to low energies, and not sufficient to provide isotopic resolution for helium. However, elemental resolution for the more abundant elements can still be achieved (see Table I).

F. Electronics and Data Handling

Fast analog electronics provide the basic counting rate information needed for the computation of absolute fluxes,

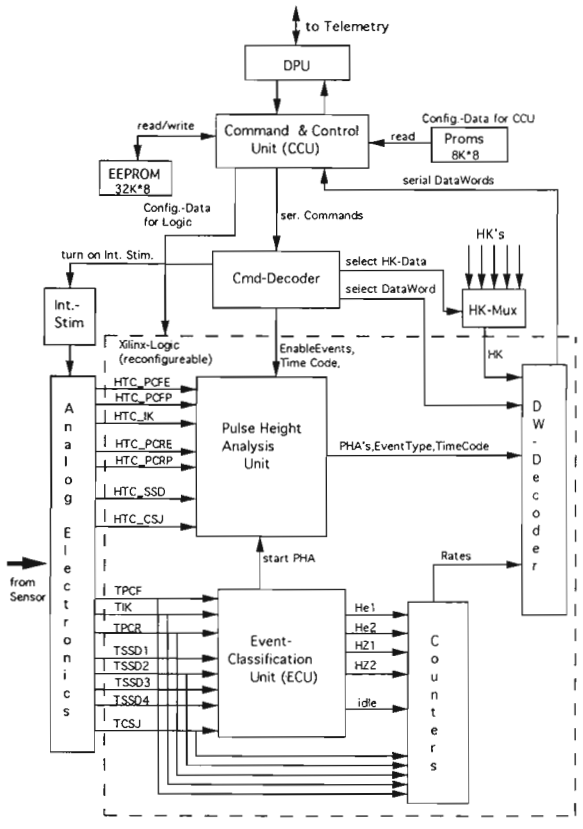

Fig. 3. Schematic block diagram of the HILT electronics.

while pulse height analysis contains the detailed energy, mass, position, and time information. All the information is read out and accumulated in the SAMPEX digital processing unit (DPU) and transmitted from there to the mass memory of the spacecraft data system [19].

The instrument analog electronics are designed to cover the energy range from a few MeV/nucleon to 5000 MeV total energy loss in the detector arrays for the elements in the mass range from helium to iron. A simplified block diagram is shown in Fig. 3. The signals from the analog electronic are processed in the Event Classification Unit (ECU) and Pulse Height Analysis Unit (PHAU). Both units are implemented in two XILINX 3090 programmable gate arrays. The configuration program for these units is stored in an EEPROM and loaded after every startup by the third XILINX, the Command and Control Unit (CCU). The CCU provides also the interface to the digital processing unit (see also [19]).

1) Rate Data: The rate data are derived from fast thresholds at the output of ten charge-sensitive amplifier chains. These thresholds are used in the Event Classification Unit (ECU) to define four rate channels, two for helium and two for $Z \geq 6$ ions (Basic Rates). These rates are accumulated and readout by the Digital Processing Unit (DPU) every 6 seconds. In addition to the Basic Rates, the lowest thresholds of all detector elements used in the ECU, three diagnostic rates on coincidence conditions, and the idle time of the system (to be used for dead time corrections), are monitored with reduced time resolution. These monitor rates provide integral measurements of the particle distribution and information on the health and safety of the experiment. Furthermore, low thresholds on the IC, PCR, and SSD1-4 channels are directly fed into the DPU and read out every 0.1 s providing information on particle intensity variations on a much shorter time scale. The monitor and high time resolution rates from the front and rear proportional counter are also sensitive to electrons which are scattered in the front foil or in the solid state detector array and then penetrate the ionization chamber at oblique angles. However, because of the low efficiency of the electron response (2×10^{-4}, see also Table II), these rates will be dominated by electrons only during passes of the electron radiation belts of the Earth.

The coincidence logic in the ECU can be switched by command into a mode where signals from the PC-IC system are not included in the coincidence conditions (High Energy Mode). This mode will be used after the Isobutane counter gas is all used up and thus will recover the SSD-CsI coincidence measurement. However, because no path-length correction is possible without the proportional counter system, the elemental resolution will be degraded and only allow the resolution of element groups (e.g., He, CNO, see also Table I). With the Isobutane system in operation, this mode can also be used to obtain measurements of proton spectra. A summary of the response of all the rate channels is provided in Table II.

2) Pulse Height Event Data: The signals of all channels are pulse height analyzed. The information on the signal amplitudes, the event type, the SSD row triggered and the time of observation is transmitted as one pulse height event. The DPU has complete control of the HILT event readout and a priority algorithm ensures that for high rates all four event types, corresponding to the four Basic Rates, would be analyzed at about the same rate. The total number of PHA events read out per sensor is limited by the memory allocation in the solid state recorder of the spacecraft (see also [19]), the maximum event rate can be selected by ground command and will be $\approx$10 events per second for each event type.

3) Instrument Performance: The position (and directional) resolution depends on the resolution of the drift time measurement and on the energy loss in the front and rear proportional counters. The resolution therefore depends on particle type and energy and is increasing with particle mass and decreasing with particle energy. Table III provides typical values of the position resolution as derived from calibration measurements. Table III shows that for helium and $Z \geq 6$ ions the position resolution is limited by the resolution of the proportional counter and the size of the solid state detectors, respectively. The resulting resolution of the zenith angle for $Z \geq 6$ ions at energies < 40 MeV/nucleon is typically $< 5°$ FWHM.

The elemental resolution of the sensor depends on the resolution of the energy loss measurement in the proportional counter–ionization chamber system and on the accuracy of the trajectory determination for path length correction. Thus, the elemental resolution depends on particle type and energy (see also Table I). In Fig. 4 the energy loss in the front proportional counter (PCF) and the residual energy in the solid state detector array for carbon and oxygen in a calibration measurement have been converted into a nuclear charge scale. The data show that the nuclear charge resolution in the energy range

TABLE III
HILT POSITION RESOLUTION

Measurementz	^{4}He	^{16}O	^{40}Ar
Energy (MeV/n)	25	30	12.6
Position Resolution in Top Plane (FWHM)	(cm)	(cm)	(cm)
PCF	7.0	0.80	0.40
Drift	1.1	0.85	0.55
Position Resolution in Bottom Plane (FWHM)			
PCR	8.0	1.2	0.6
SSD	3.5	3.5	3.5

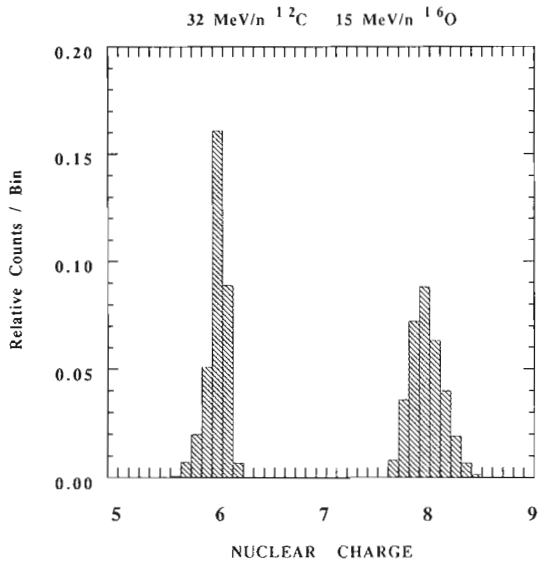

Fig. 4. Nuclear charge histogram derived from the measurement of energy loss in PCF and residual energy in SSD.

10 to 32 MeV/nucleon is $\approx$0.3 (FWHM), i.e. all elements between helium and oxygen can easily be resolved. The elemental resolution of the rear proportional counter and of the ionization chamber is similar to the one shown. This provides some redundancy because all three sections of the proportional counter–ionization chamber system can be used independently for the identification of elements.

4) Data Products: Routine data products from HILT will include time versus counting rate plots of the four Basic Rates and of selected monitor rates. These rate plots will be the basis for the selection of time periods for further detailed analysis of HILT data and for the collaborative investigation of particular events with all sensors on board SAMPEX and other spacecraft. Basic rate data and pulse height data obtained at high geomagnetic latitudes, where cutoff effects are negligible, will be used to compute absolute fluxes and energy spectra for different ions during solar particle events. Pulse height data at lower latitudes will be used to compute the trajectories of the ions in the magnetic field of the Earth to infer the ionic charge of the ions.

ACKNOWLEDGMENT

The authors would like to thank the many individuals and institutions who contributed to the design, fabrication, and test of the instrument. We are also grateful for the devoted work of the technical staff and the workshops at the Max-Planck-Institut für Extraterrestrische Physik and at The Aerospace Corporation.

REFERENCES

[1] D. Hovestadt, B. Klecker, P. Laeverenz, E. Seidenschwang, G.M. Mason, P.D. Bedini, G. Gloeckler, D.C. Hamilton, J.B. Blake, and D. Chenette, "Experiment for charge determination of cosmic rays of interplanetary and solar origin on the space shuttle," *Proc. 20th Internat. Cosmic Ray Conf. (Moscow),* vol. 4, p. 406, 1987.
[2] D.V. Reames, "Energetic particles from impulsive solar flares," *Ap. J. Supp.,* vol. 73, p. 235, 1990.
[3] G.M. Mason, D.V. Reames, B. Klecker, D. Hovestadt, and T.T. von Rosenvinge, "The heavy ion compositional signature in ^{3}He solar particle events," *Ap. J.,* vol. 303, p. 849, 1986.
[4] E. Möbius, M. Scholer, D. Hovestadt, B. Klecker, and G. Gloeckler, "Comparison of helium and heavy ion spectra in ^{3}He-rich solar flares with model calculations based on stochastic Fermi acceleration in Alfvén turbulence," *Ap. J.,* vol. 259, p. 397, 1982.
[5] D.N. Baker, G.M. Mason, O. Figueroa, G. Colon, J.G. Watzin, and R.M. Aleman, "An overview of the Solar, Anomalous, and Magnetospheric Particle Explorer (SAMPEX) Mission," *IEEE Trans. Geosci. Remote Sensing.,* vol. 31, p. 531–541, May 1992.
[6] G.M. Mason, D.C. Hamilton, P.H. Walpole, K.F. Heuermann, T.L. James, M.H. Lennard, and J.E. Mazur, "LEICA: A low energy ion composition analyzer for the study of solar and magnetospheric heavy ions," *IEEE Trans. Geosci. Remote Sensing.,* vol. 31, p. 549–556, May 1992.
[7] A. Luhn, B. Klecker, D. Hovestadt, and E. Möbius, "The mean ionic charge of silicon ^{3}He-rich solar flares," *Ap. J.,* vol. 317, p. 951, 1987.
[8] D. Hovestadt, *et al.,* "The nuclear and ionic charge distribution particle experiments on the ISEE-1 and ISEE-C spacecraft," *IEEE Trans. Geosci. Electr.,* vol. GE-16, p. 166, 1978.
[9] G. Gloeckler, "Compositions of energetic particle populations in interplanetary space," *Rev. Geophys. Space Phys.,* vol. 17, p. 569, 1979.
[10] L.A. Fisk, B. Kozlovsky, and R. Ramaty, "An interpretation of the observed oxygen and nitrogen enhancements in low-energy cosmic rays," *Ap. J. (Letters),* vol. 190, p. L39, 1974.
[11] J.R. Jokipii, "Particle acceleration at a termination shock 1. Application to the solar wind and the anomalous component," *J. Geophys. Res.,* vol. 91, p. 2929, 1986.
[12] R.B. McKibben, "An experimental test for the charge state of the "anomalous" helium component," *Ap. J. (Letters),* vol. 217, p. L113, 1977.
[13] B. Klecker, D. Hovestadt, G. Gloeckler, and C.Y. Fan, "On the charge state of the anomalous oxygen component," *Geoph. Res. Lett.,* vol. 7, p. 1033, 1980.
[14] K. Oschlies, R. Beaujean, and W. Enge, "On the charge state of anomalous oxygen," *Ap. J.,* vol. 345, p. 776, 1989.
[15] R.K. Singh, *et al.,* "Ionization states of the anomalous cosmic rays," *Ap. J.,* vol. 374, p. 753, 1991.
[16] J.H. Adams, Jr., *et al.,* "The charge state of the anomalous component of cosmic rays," *Ap. J. (Letters),* vol. 375, p. L45–L48, 1991.
[17] W.R. Cook *et al.,* "MAST: A mass spectrometer telescope for studies of the isotopic composition of solar, anomalous, and galactic cosmic ray nuclei," *IEEE Trans. Geosci. Remote Sensing.,* vol. 31, p. 557–564, 1992.
[18] N.L. Grigorov, *et al.,* "Evidence for trapped anamolous cosmic ray oxygen ions in the inner magnetosphere," *Geophys. Res. Letters,* vol. 18, p. 1959, 1991.
[19] D.J. Mabry, S.J. Hansel, and J.B. Blake, "The SAMPEX data processing unit (DPU)," *IEEE Trans. Geosci. Remote Sensing.,* vol. 31, p. 572–574, 1992.

Berndt Klecker received the Ph.D. degree in Physics from the Technical University of Munich, Germany, in 1978.

He worked at the Max-Planck-Institut für Extraterrestrische Physik at Garching, Germany, since 1976 specializing on experimental and theoretical cosmic ray physics. He was collaborator and coinvestigator on many energetic particle experiments on several magnetospheric and interplanetary spacecraft (e.g., GRS-A AZUR, ESRO-IV, IMP-7 and -8, ISEE-1, ISEE-3/ICE, AMPTE, SAMPEX, SOHO, CLUSTER).

Dietrich Hovestadt received the Diploma in Physics at the University of Hamburg, in 1960 and the Ph.D. degree in nuclear physics at the Technical University Munich, in 1964.

In 1964 he joined the Max-Planck-Institut for Physik and Astrophysik in Munich, working as the head of the energetic particle group. Since 1966 he has worked experimentally in the field of magnetospheric particle, solar, and interplanetary cosmic ray physics. He participated in many satellite-borne experiments and was principal investigator on several of them.

Manfred Scholer received the Ph.D. degree in physics from the Technical University Munich in 1969.

During 1969–1970 he held a ESA/NASA fellowship at the California Institute of Technology. He joined the Max-Planck-Institut für Extraterrestrische Physik in 1971 as a staff member and became group leader in 1985. He was Collaborator on the spacecraft missions AZUR GRS-1, ESRO IV, IMP-7, IMP-8, and Co-Investigator on ISEE-1, ISEE-3, and AMPTE-IRM. His current interests are numerical simulations of processes in space plasmas.

Dr. Scholer is a member of AGU and the German Physics Society.

H. Arbinger, photograph and biography not available at the time of publication.

M. Ertl, photograph and biography not available at the time of publication.

H. Kästle, photograph and biography not available at the time of publication.

E. Künneth, photograph and biography not available at the time of publication.

P. Laeverenz, photograph and biography not available at the time of publication.

E. Seidenschwang, photograph and biography not available at the time of publication.

J. B. Blake, photograph and biography not available at the time of publication.

N. Katz, photograph and biography not available at the time of publication.

D. Mabry, photograph and biography not available at the time of publication.